AIAA JOURNAL
Vol. 41, No. 9, September 2003

Turbulence Modeling Applied to Flow over a Sphere

George Constantinescu,* Matthieu Chapelet,† and Kyle Squires‡
Arizona State University, Tempe, Arizona 85287-6106

Numerical simulations of the subcritical flow over a sphere are presented. The primary aim is to compare prediction of some of the main physics and flow parameters from solutions of the unsteady Reynolds-averaged Navier–Stokes (URANS) equations, large-eddy simulation (LES), and detached-eddy simulation (DES). URANS predictions are obtained using two-layer k–ε, k–ω, v^2–f, and the Spalart–Allmaras model. The dynamic eddy viscosity model is used in the LES. DES is a hybrid technique in which the closure is a modification to the Spalart–Allmaras model, reducing to RANS near solid boundaries and LES in the wake. The techniques are assessed by evaluating simulation results against experimental measurements, as well as through their ability to resolve time-dependent features of the flow related to vortex shedding. Simulation are performed at a Reynolds number of 10^4, where laminar boundary-layer separation occurs at approximately 83 deg. With the exception of two-layer k–ε, RANS predictions of the streamwise drag are in reasonable agreement with measurements. The pressure and skin-friction coefficients along the sphere are adequately predicted by the RANS models, with DES and LES results in better agreement with measurements in the aft region. Profiles of the mean velocity and turbulent kinetic energy in the near wake from all of the techniques are similar. The nearly axisymmetric URANS solutions predict the value of the main shedding frequency, albeit at substantially reduced amplitude compared to the LES and DES. DES compares favorably with LES in that both techniques resolve eddies down to the grid scale in the wake and are better able to capture unsteady phenomena, including formation of Kelvin–Helmholtz instabilities in the detached shear layers and the associated high frequency in the flow.

I. Introduction

A. Background

An important class of separated flows are those in which the location of flow detachment is not fixed by the geometry and are not subject to external effects that are used to force unsteadiness, as occurs for many bluff body flows. The main interest of the present study is prediction of the flow around a sphere in the subcritical regime, a complex case characterized by large-scale vortex shedding, transitional shear layers, and a turbulent wake with random and periodic Reynolds stresses of comparable magnitudes. Simulation of the flow around a sphere is then an important benchmark for techniques used to predict massively separated flows.

Most engineering predictions of separated flows are obtained from solutions of the Reynolds-averaged Navier–Stokes (RANS) equations, with an increasing interest in the use of large-eddy simulation (LES). As discussed by Spalart,[1] there are important criteria that RANS models should satisfy to yield accurate predictions of complex flows: Models should correctly predict the growth and separation of the boundary layers and accurately capture the Reynolds stresses after separation. For the sphere considered in this work, boundary layers are laminar at separation (subcritical regime), with transition occurring in the separated shear layers. Accurate prediction of separation in this case then requires that in the laminar boundary layers (and, in general, in the laminar regions of the flow), turbulence models should accept vanishing solutions for the Reynolds stresses, or at least small values without influence on the turbulent layers. In addition, the behavior of the models at turbulent/nonturbulent interfaces should allow the contamination of a laminar shear layer by contact with a strongly turbulent layer, and models should be relatively insensitive to freestream values of the turbulence variables.

Satisfaction of the first requirement described, adequate prediction of boundary-layer growth and separation, generally requires closure models that resolve the near-wall flow, rather than approaches that employ wall functions. Previous work indicates, for example, the importance of resolving the viscous wall layer to obtain shedding solutions in RANS calculations.[2,3] Each of the RANS approaches considered in this work resolve the near-wall region and can be integrated all of the way to the wall: two-layer k–ε (Ref. 4) low Reynolds number k–ω (Ref. 5), v^2–f (Ref. 6), and Spalart–Allmaras[7] (S-A). These models invoke the Boussinesq approximation, by the use of one or more equations to determine the isotropic eddy viscosity, and, therefore, provide a crude representation of the anisotropy of the Reynolds stresses. Although often sufficient in attached regions not far from the thin shear layer approximation, it is difficult to satisfy the second criterion outlined, accurate capture of the Reynolds stresses after separation, by the use of RANS approaches that employ the Boussinesq approximation. The utility of more complex RANS models, for example, Reynolds-stress closures, for satisfaction of this requirement remains a subject of debate.[1]

Previous applications of these models to separated flows include prediction of the flow around triangular cylinders using k–ε (Ref. 8) and v^2–f (Ref. 3), rectangular cylinders using k–ε (Refs. 9 and 10), circular cylinders using S-A,[11,12] and two-dimensional airfoils using S-A.[13] Averaging of the shedding solution in a RANS calculation typically yields a significant fraction of the Reynolds stress, in turn lessening the burden on the turbulence model. These studies show that it is possible to resolve time-periodic shedding solutions with a wake frequency generally comparable to the lowest frequency measured in experiments. The amplitude modulation of the actual shedding is difficult to represent, however, and is one cause of the sometimes poor predictions of integral quantities such as the drag.[1]

There are relatively few RANS or unsteady RANS (URANS) predictions of spheres in the turbulent regime. Drikakis[14] computed the flow past a sphere using an artificial compressibility method and grid sizes up to about 58,000 grid volumes. Steady-state, that is, time-independent, subcritical, and supercritical flows were computed with the Baldwin–Lomax[15] and the k–ε model. Predictions of the pressure coefficient C_p for the subcritical case were in reasonable

Received 12 October 1999; revision received 19 February 2003; accepted for publication 12 March 2003.

*Research Engineer, Mechanical and Aerospace Engineering Department; currently Research Engineer, Iowa Institute Hydraulics Research—Hydroscience and Engineering, University of Iowa, 100 C. Maxwell Stanley Hydraulics Laboratory, Iowa City, IA 52242-1585.

†Research Assistant, Mechanical and Aerospace Engineering Department.

‡Professor, Mechanical and Aerospace Engineering Department.

agreement with measurements before separation, though predictions of the pressure coefficient in the wake were rather poor. For the supercritical flow, the pressure coefficient was inaccurate over most of the sphere, which results in large errors in the drag.

Techniques that resolve more flow details, such as LES, are attractive for massively separated flows because a significant fraction of the turbulent motions are not modeled, instead being directly resolved on the grid. LES then provides a powerful approach for capturing the Reynolds stresses in separated regions, where the stresses are dominated by the geometry-dependent large eddies. Tomboulides et al.[16] used LES (in addition to direct numerical simulations at lower Reynolds numbers[17] to predict the wake behind a sphere using a subgrid model based on renormalization group theory. Predictions were obtained at a Reynolds number of 2×10^4, where there is a laminar boundary-layer separation. Tomboulides et al.[16] resolved the higher frequencies present in time histories of the streamwise drag caused by instabilities in the detached shear layers. These investigators also obtained predictions of the drag that were in good agreement with measurements. Although not exhaustive, this study demonstrates that resolution of features related to vortex shedding and three-dimensionality of the flow are important to the capture of unsteady effects. Such effects are more difficult to resolve by the use of closure models, which parameterize all scales of motion as in Reynolds-averaged methods.

LES, despite requiring less empiricism than RANS, carries a high computational cost when used to resolve thin features of fully turbulent flows.[18,19] To combine the most favorable aspects of RANS and LES, Spalart et al.[19] proposed a hybrid technique known as detached-eddy simulation (DES), essentially reducing to RANS near solid boundaries and LES away from the wall. The closure is based on a simple modification to the S–A model and takes advantage of the usually adequate performance of RANS models in the thin shear layers where these models are calibrated. In separated regions where the flow is far from the thin shear layer approximation, an LES treatment is used to resolve time-dependent structures that are not treated as well with RANS. Most of the stress in the LES region is resolved, rather than modeled, and stress anisotropies are calculated directly. DES and LES predictions are used in the present investigations to provide a basis for evaluation of unsteady effects predicted by RANS models.

B. Objectives and Approach

The main goal of this paper is to evaluate the performance of some of the leading RANS models by the use of predictions of the subcritical flow over a sphere: two-layer k–ε, k–ω, $\overline{v^2}$–f, and S–A. Predictions are evaluated against the experimental measurements of Achenbach,[20] as well as results from DES and LES. The present contribution focuses on a Reynolds number in the subcritical regime, $Re = 10^4$, where there is a laminar boundary-layer separation from the sphere surface. The laminar separation relaxes resolution requirements near the surface, in turn permitting performance of whole-domain LES using a grid of approximately 5×10^5 points.

RANS predictions of the unsteady flow are obtained from numerical solution of the time-dependent Navier–Stokes equations. One of the challenges for the RANS models is the application outside their calibration range, that is, in a massively separated flow that is far from the thin shear layers where the model constants in the turbulent transport equations are calibrated. A priori, it might be expected that this would result in poor predictions. However, URANS results discussed in Sec. III show that predictions of quantities such as the pressure coefficient and skin friction along the sphere are mostly adequate. The main deficiency associated with the URANS simulations is related to the more general problem that Reynolds averaging suppresses much useful information from the solution. For the subcritical flow around the sphere considered in this study, frequencies associated with the main instability modes and the energy content of these frequencies are not well resolved, and the URANS solutions become essentially axisymmetric and nearly steady. This behavior differs from related applications of URANS methods to massively separated flows such as the circular cylinder, in which time-periodic shedding solutions are obtained.[12] As discussed in Sec. III, the different character of the URANS solutions of the sphere compared to other cases such as the flow around a circular cylinder might be attributed in part to the reduced coherence of the shed structures in the wake.

Unlike RANS approaches, the role of the turbulence model is less dominant in LES and DES where the large scales, which contribute strongly to unsteady effects, are resolved. Consequently, a refined evaluation of the URANS is possible by bringing out aspects of these calculations relative to the LES and DES predictions. Note that because boundary-layer separation is laminar, the DES predictions constitute an LES away from the boundary performed in this investigation with a one-equation transport model for the subgrid-scale eddy viscosity. An evaluation of the DES is, therefore, possible in the subcritical regime via comparison to the LES predictions obtained with a more established approach. For supercritical flows that experience turbulent boundary-layer separation, a similar evaluation of DES predictions is somewhat more ambiguous due to the need to model the wall layer in LES.

In the following section, the numerical method, boundary conditions, and turbulence models are summarized, along with discussion of aspects concerning validation of the simulations. URANS, LES, and DES results are then presented along with comparisons to experimental measurements. The main focus in Sec. III is on prediction by these techniques of the overall parameters of engineering interest, as well as some unsteady features of the flow. Conclusions and recommendations are presented in Sec. IV.

II. Simulation Overview

A. Numerical Approach

In the present study, the incompressible flow around a sphere is computed with a fractional step method. The governing equations are transformed to generalized curvilinear coordinates with the primitive velocities and pressure retained as the dependent variables. The base numerical method was previously employed for computation of steady flows.[21,22] Extension to time-accurate calculations was performed with a double-time-stepping algorithm as described by Johnson[23] and is summarized hereafter.

Within a physical time step, the momentum and turbulence model equations are integrated in pseudotime using a fully implicit algorithm. In the first step of the fractional step method, an intermediate velocity field is obtained by advancing the convection and diffusion terms using an alternate direction implicit approximate factorization scheme. The intermediate field is obtained with the current pressure field and does not satisfy the continuity equation. A Poisson equation is then solved for the pressure, and the resulting solution is used to update the intermediate velocities so that continuity is satisfied. Advancement in pseudotime is continued until a converged solution of the equations is obtained. Local time-stepping techniques are used to accelerate the convergence of the resulting system of equations. Source terms in the turbulence-model equations are also treated implicitly.

All terms in the pressure Poisson equation are discretized with second-order accurate central differences. Odd–even decoupling in the pressure field, associated with the discretization of the equations on nonstaggered grids, is circumvented through use of the operator developed by Sotiropoulos and Abdallah.[24] The momentum and turbulence transport equations are discretized using either second- or fifth-order-accurate upwind differences for the convective terms, whereas all other operators are calculated using second-order central differences. The overall discretization scheme is second-order accurate in space, including at the boundaries. Effects of the order of upwinding and the dissipation associated with the odd–even decoupling algorithm are discussed in Sec. II.D.

Solutions are obtained on a domain that extends from the sphere surface ($r = 0.5D$ where D is the sphere diameter) to 15 diameters in the radial direction. The governing equations are solved on an O–O grid with (r, ϕ, θ) the radial, polar, and azimuthal directions, respectively. The conditions at the upstream boundary ($r = 15D$, $0 < \phi < 0.55\pi$) consist of a uniform velocity. Turbulence variables at the inflow boundary were set to their

threshold values [$k/U^2 = 10^{-8}$, $\varepsilon/(U^3/D) = 10^{-6}$, $\omega D/U = 10^{-1}$, and $\nu_t/(UD) = 10^{-8}$]. The velocity components and turbulence variables at the downstream boundary ($r = 15D$, $0.55\pi < \phi < \pi$) are obtained with second-order extrapolation from the interior of the domain. No-slip conditions on the sphere surface are imposed. The pressure boundary condition on the sphere and at the upstream and downstream boundaries are obtained from the surface-normal momentum equation. Periodic boundary conditions are imposed on all variables in the azimuthal direction. On the polar axes, ($\phi = 0, \pi$), the variables (pressure, velocity, and turbulence quantities) are obtained by averaging over the azimuth a second-order accurate extrapolation of these variables.

The calculations were carried out on a mesh of about 450,000 grid nodes ($101 \times 42 \times 101$ points in the r, θ, and ϕ directions) with the first point off the wall situated at about $r^+ = 0.2$, and about eight points within $r^+ < 10$ (based on an estimate of the friction velocity of 0.04). The maximum grid spacing near the sphere surface is roughly nine wall units in the polar direction and 42 wall units in the azimuth (at $\phi = 0.5\pi$). The effect of grid refinement is discussed in Sec. II.D. For the k–ε model, turbulent boundary-layer profiles of k and ε were initially prescribed near the sphere surface. The steady-state k–ε solutions were subsequently used as the initial fields for calculations performed with other turbulence models.

The equations were advanced with a physical time step of $0.02D/U$, where U is the freestream velocity. This insured approximately 220 time steps per cycle, corresponding to the main shedding frequency. The convergence criterion at every time step was that the maximum value of the velocity and pressure residuals should be smaller than 10^{-4}. This insured a reduction of more than two orders of magnitude for the norm of the velocity components to reach incompressibility at each physical time step, and yielded an adequate damping of errors throughout the entire domain. An average of about 60 subiterations were used to converge the solution per physical time step.

B. Turbulence Models: RANS

URANS solutions are obtained by solving the Reynolds-averaged and turbulence model equations in a time-accurate fashion. As the grid is refined, the turbulence model will continue to dominate the flow, and, consequently, the quality of the RANS solution will remain strongly dependent on the turbulence model. Four turbulence models are investigated in the URANS:

1) The first model investigated is the two-layer k–ε. The two-layer k–ε model of Chen and Patel[4] is straightforward in implementation and has been applied to prediction of a wide range of flows.[25,26] Two-layer k–ε reduces in the inner layer to a simple one-equation model, requiring an additional parameter, the matching distance between the two-layers, to which the solution for flows at low Reynolds numbers can be sensitive.[22] The length scale applied in the inner layer to determine the dissipation rate and eddy viscosity is a function of the turbulence Reynolds number, $k^{1/2}y/\nu$ and is inappropriate for the prediction of laminar separation. It should be expected, therefore, that the two-layer model will be inadequate for the subcritical regime of the sphere, as will be illustrated in Sec. III. The principal motivation for application of the model in the present investigation is for generation of reasonable initial fields for solutions performed with other turbulence models.

2) The next model investigated is the k–ω. The low-Reynolds-number version of the k–ω model of Wilcox[5] typically predicts adverse-pressure-gradient boundary layers more accurately than its counterpart k–ε formulation at no additional computing cost.[5,27] RANS predictions of external flows using k–ω are known, however, to be sensitive to freestream values of the turbulence variables, especially in the near wake. The implementation of boundary conditions for k and ω at solid surfaces is trivial.

3) The third model investigated is the $\overline{v^2}$–f. The $\overline{v^2}$–f model of Durbin[6] supplements k–ε with one additional transport equation (for v^2) and an elliptic relaxation equation. The model has been successfully applied to prediction of equilibrium and nonequilibrium flows.[3] An issue is the computational cost of the model (~20% increase in CPU time compared to two-equation models) and the implementation of boundary conditions for the turbulent quantities at the wall.

4) The fourth model investigated is the S–A model. The S–A model[7] computes the eddy viscosity by the use of a single transport equation. The low-Reynolds-number version of the model possesses favorable numerical characteristics in terms of near-wall resolution and stiffness properties. Specification of the boundary condition at the wall for the modified eddy viscosity is trivial.

Each of the models just summarized are linear eddy-viscosity closures and do not account for effects such as the misalignment between the turbulent stress and strain rate, presume equilibrium, etc. In addition, the models are calibrated in flows that are close to the thin shear layer approximation. Application of these models, all of which resolve the wall layers, to the time-dependent prediction of a complex three-dimensional flow far from their calibration range, is important to assessing methods used to predict other flows encountered in applications.

C. Turbulence Models: LES and DES

In LES, the subgrid-scale (SGS) stress is closed by the use of the dynamic eddy viscosity model.[28] In the dynamic approach, the resolved scales are explicitly filtered and the Germano identity is used to compute the subgrid eddy viscosity. The dynamic procedure possesses the correct asymptotic behavior near solid surfaces and differentiates between laminar and turbulent regions of the flow, without damping or intermittency functions.

In the dynamic procedure, a "test filter" is applied at coarser resolution to obtain the "test-field" stress. By the use of the Germano identity, an expression may be developed for calculation of model coefficients. When the flowfield is sampled, a mechanism is provided for dynamic models to respond to changes in the turbulence due to perturbations in the flow. As a consequence, some nonequilibrium effects are accounted for, despite the use of an isotropic eddy viscosity model. The Smagorinsky model is used as the base in this work, and the dynamic procedure yields a coefficient that varies in space and time. Test filtering is applied in the statistically homogeneous azimuthal direction with the filter width equal to two times the local grid spacing. Although it would also be possible to filter over the other dimensions locally, test filtering only over homogeneous directions offers theoretical advantages in the dynamic formulation.[29] To avoid numerical instability, the SGS viscosity obtained after the model coefficient is averaged is also constrained to be positive through truncation to zero of any negative values.

The DES formulation used in this study is based on a modification to the S–A model such that the closure reduces to RANS in boundary layers and to LES away from the wall.[19] The modification is a redefinition of the length scale of the destruction term in the eddy viscosity transport equation, written hereafter without the trip terms that were not used in the present simulations:

$$\frac{\mathrm{D}\tilde{\nu}}{\mathrm{D}t} = c_{b1}\tilde{S}\tilde{\nu} + \frac{1}{\sigma}\left[\nabla\cdot((\nu+\tilde{\nu})\nabla\tilde{\nu}) + c_{b2}(\nabla\tilde{\nu})^2\right] - c_{w1}f_w\left[\frac{\tilde{\nu}}{d}\right]^2 \quad (1)$$

where $\tilde{\nu}$ is the working variable,

$$\tilde{S} \equiv S + (\tilde{\nu}/\kappa^2 d^2) f_{v2}, \qquad f_{v2} = 1 - \chi/(1 + \chi f_{v1}) \quad (2)$$

and S is the magnitude of the vorticity. The eddy viscosity ν_t is obtained from

$$\nu_t = \tilde{\nu} f_{v1}, \qquad f_{v1} = \chi^3/\left(\chi^3 + c_{v1}^3\right), \qquad \chi \equiv \tilde{\nu}/\nu \quad (3)$$

where ν is the molecular viscosity. The function f_w is given by

$$f_w = g\left[\frac{1 + c_{w3}^6}{g^6 + c_{w3}^6}\right]^{\frac{1}{6}}, \qquad g = r + c_{w2}(r^6 - r), \qquad r \equiv \frac{\tilde{\nu}}{\tilde{S}\kappa^2 d^2} \quad (4)$$

The wall boundary condition is $\tilde{\nu} = 0$. The constants are $c_{b1} = 0.1355$, $\sigma = \frac{2}{3}$, $c_{b2} = 0.622$, $\kappa = 0.41$, $c_{w1} = c_{b1}/\kappa^2 + (1 + c_{b2})/\sigma$, $c_{w2} = 0.3$, $c_{w3} = 2$, and $c_{v1} = 7.1$. The DES formulation is obtained

when the distance to the nearest wall d, is replaced by $\widetilde{d}$, where $\widetilde{d}$ is defined as

$$\widetilde{d} \equiv \min(d, C_{\mathrm{DES}}\Delta) \qquad \text{with} \qquad \Delta \equiv \max(\Delta x, \Delta y, \Delta z) \quad (5)$$

Near walls, Δ is larger than d, and the standard S–A model is obtained. Consequently, prediction of boundary-layer separation is determined in the RANS mode of DES. Away from solid boundaries, the closure is a one-equation model for the SGS eddy viscosity. The additional model constant $C_{\mathrm{DES}} = 0.65$ was calibrated with simulations of homogeneous turbulence[13] and is used without modification in this study. In both the LES and DES predictions presented here, the convective terms were discretized by the use of fifth-order, upwind-biased finite differences.

D. Simulation Validation

Variants of the flow solver used in this study employing several RANS closures have been tested extensively for prediction of steady flows and accurately predicted complex three-dimensional laminar and turbulent flows.[21,22,25,30,31] Preliminary validation of the time-accurate solver was performed through calculation of the flow past a sphere in the laminar, unsteady regime ($Re = 300$) and comparison of drag predictions (both streamwise and lateral) against published results.

At $Re = 300$, vortices are shed regularly from the sphere. By the use of the solver employed in the current study, predictions of the drag coefficient C_d and its rms amplitude are 0.6556 and 0.0032, respectively. Johnson and Patel[32] obtained 0.656 and 0.0035, and Tomboulides et al.[16] computed 0.671 and 0.0028, respectively. Roos and Willmarth[33] measured $C_d = 0.629$. The mean value and the amplitude of the resultant lateral-force coefficient were 0.065 and 0.017 with the present method, and 0.069 and 0.016 in Ref. 32. Predictions of the shedding Strouhal number are 0.136, which agrees well with the corresponding values obtained by Johnson and Patel[32] and Tomboulides et al.[16] of 0.137 and 0.136, respectively. Sakamoto and Haniu[34] measured a value of the Strouhal number in the range of 0.15–0.16 at $Re = 300$. Simulation results showed that the second-order extrapolation used at the downstream boundary did not negatively affect the unsteady flow, that is, no spurious oscillations nor odd–even decoupling were detected near the boundary or within the computational domain. Further validation of the time-accurate solver for turbulent flow simulations is provided in the results section, where comparison with experimental data is provided for the main parameters describing the unsteady shedding.

Grid sensitivity was assessed for the RANS calculations when the mesh was refined in the polar direction, with a grid of $151 \times 42 \times 101$ points. Calculations were carried out using the k–ω and S–A models. Solutions on the finer grid agreed well with those on the coarser mesh, the pressure coefficient and skin friction along the sphere differing by less than 5% on the coarse and fine grids. Grid dependence for the eddy-resolving calculations was evaluated by the use of DES predictions on two grids in which the azimuthal resolution was increased by a factor of two: DES-coarse grid (DES-CG) DES-finer grid (DES-FG). The mean streamwise velocity $\widetilde{V}_1$ and resolved-scale turbulence kinetic energy K in the near wake are shown in Fig. 1. The mean velocity exhibits little variation on the two grids, with a slightly higher centerline velocity on the coarse grid at $x/D = 1.2$. Predictions of K for these cases are also similar to turbulence kinetic energy levels slightly larger close to the sphere ($x/D = 0.6$) on the fine grid, consistent with the finer mesh supporting a larger range of scales. The mean pressure and skin-friction distributions over the sphere, shown in Figs. 2 and 3 for the two grids, are also in good agreement. Correspondingly, the predictions of the streamwise drag are similar, differing in C_d by 1.5% in between the two computations. The Strouhal numbers associated with the main shedding for DES-FG and DES-CG were 0.190 and 0.200, respectively. The Strouhal number ranges associated with the shear-layer instabilities showed more variation, ranging between 1.6 and 2.4 for the fine grid, and between 1.9 and 2.1 for the coarse grid. In addition, the higher-frequency range on the fine grid was more energetic.

The effect of numerical dissipation on the DES and LES solutions was investigated by Constantinescu and Squires.[35] Results in that

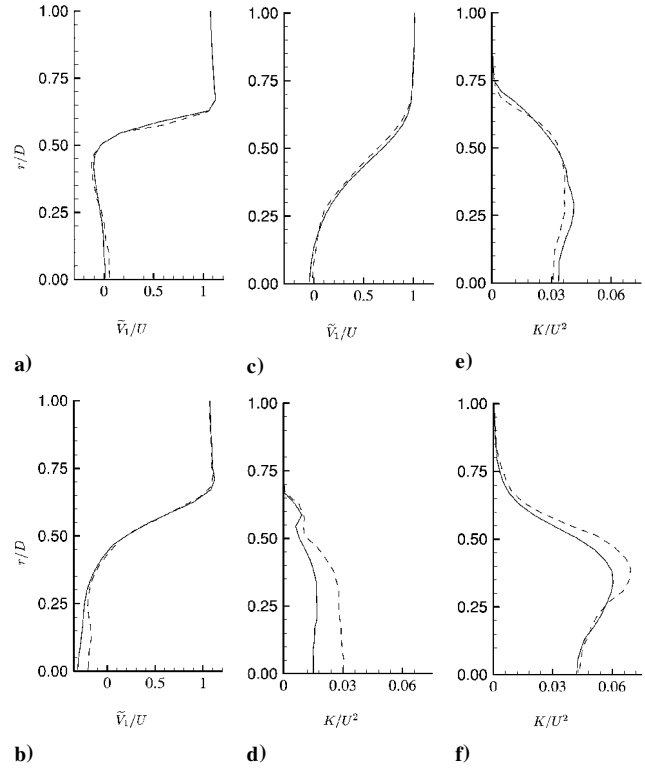

Fig. 1 Mean streamwise velocity (upper figures) and resolved-scale turbulence kinetic energy (lower figures) in the near wake: ——, DES-CG; – – –, DES-FG; a) and d) $x/D = 0.6$, b) and e) $x/D = 1.2$, and c) and f) $x/D = 2.0$.

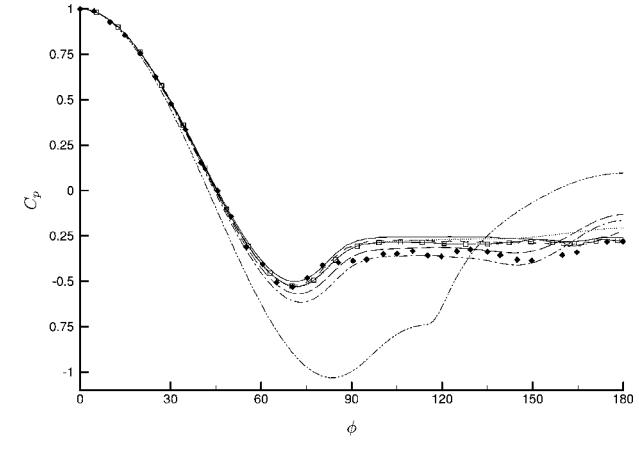

Fig. 2 Pressure coefficient (averaged over the azimuthal coordinate): – – –, k–ω; –·–·–, k–ε; · · · ·, v^2–f; –·–, S–A; - - - -, LES; □, DES-CG; ——, DES-FG; and ♦, Achenbach.[20]

study show that, although the employment second-order upwind discretizations for the convective terms was sufficient for the RANS solutions, use of higher-order discretizations (fifth-order upwind biased differences) was important for resolving the spectral distribution of energy and shedding parameters at higher wavelengths and frequencies. Investigations into the role of the model and the influence of numerical dissipation were also conducted when calculations that did not explicitly include the subgrid model were included. Solutions became numerically unstable in such calculations, in turn providing evidence of the importance of the subgrid models to obtaining convergent, and accurate, predictions. In general, these features concerning the order of the upwind scheme, role of the subgrid model, etc., are consistent with related LES studies.[36] Although the nondissipative nature of centered methods are preferable for turbulence simulations, low-order schemes for the convective operators can suffer from dispersive errors, for example, as can occur on stretched grids. This complicates application of these methods for

use in turbulence-resolving simulations at high Reynolds numbers and in complex geometries.

In spite of the limitations, higher-order upwind-biased methods have yielded reasonable predictions of the mean flow and low-order statistics in previous LES studies.[13,36,37] Previous work by Johnson and Patel[32] using the numerical method employed in this study has shown a negligible effect of the artificial dissipation in the Poisson equation on the formal order of accuracy of the method. In the present work, the spectral content at high frequencies is not overly damped. In addition, finer-scale features, such as the development of the Kelvin–Helmholtz instabilities in the detached shear layers, are resolved only via application of the fifth-order upwind discretization. Though not shown here, these features are not resolved using second-order upwind biased differences of the convective terms.

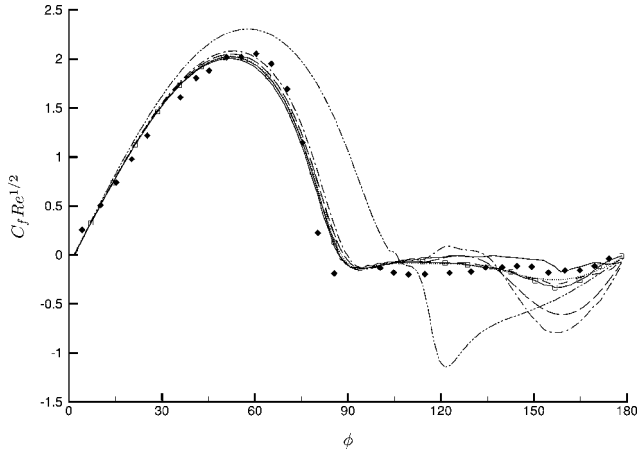

Fig. 3 Skin-friction coefficient (averaged over the azimuthal coordinate): – – –, k–ω; –···–, k–ε; · · · ·, v^2–f; –·–, S–A; - - - -, LES; □, DES-CG; ——, DES-FG; and ♦, Achenbach.[20]

III. Results

In this section, the techniques URANS, LES, and DES are assessed through comparison against measurements, as well as through intercomparison of the results obtained with each technique. The comparisons between the four URANS models and LES and DES predictions serve to evaluate the capability of these models to resolve unsteady features of the flow accurately.

In an attempt to minimize numerical uncertainties and allow a focus on the differences between the various techniques used to predict the sphere, results presented in this section were obtained with the same flow solver, grid, and boundary conditions. The momentum and turbulence-transport equations are integrated all of the way to the wall, and the viscous wall layers are adequately resolved. In turn, it should be possible to assess the predictive capabilities of the techniques independently of the effects arising from numerical resolution, because insufficient resolution of the wall layer can adversely affect the capability of a model to capture unsteady features such as vortex shedding.[2,3] Also note that the computational cost of the various models will vary, for example, increases in computational requirements for RANS closures that carry more transport equations. Simulations performed with k–ω (and k–ε) required about 15% more CPU time than calculations performed with S–A. The computational cost of v^2–f as measured in terms of CPU usage was approximately 40% greater than for simulations with S–A.

Contours of the out-of-plane vorticity component from the DES and LES in an r–ϕ plane are shown in Fig. 4. Figure 4 shows an array of vortices of varying scale in the detached shear layers. The shear layers are laminar at separation, and transition takes place over a certain distance with Kelvin–Helmholtz instabilities in the shear layers developing into vortex tubes shortly downstream of the sphere. The process is especially clear in the LES, but DES predictions also show the shear-layer vortices. (In Fig. 4 the same contour interval is used to allow direct comparison between the plots.) Vortex development is also apparent in the pressure field (not shown), where alternating regions of low and high pressure are

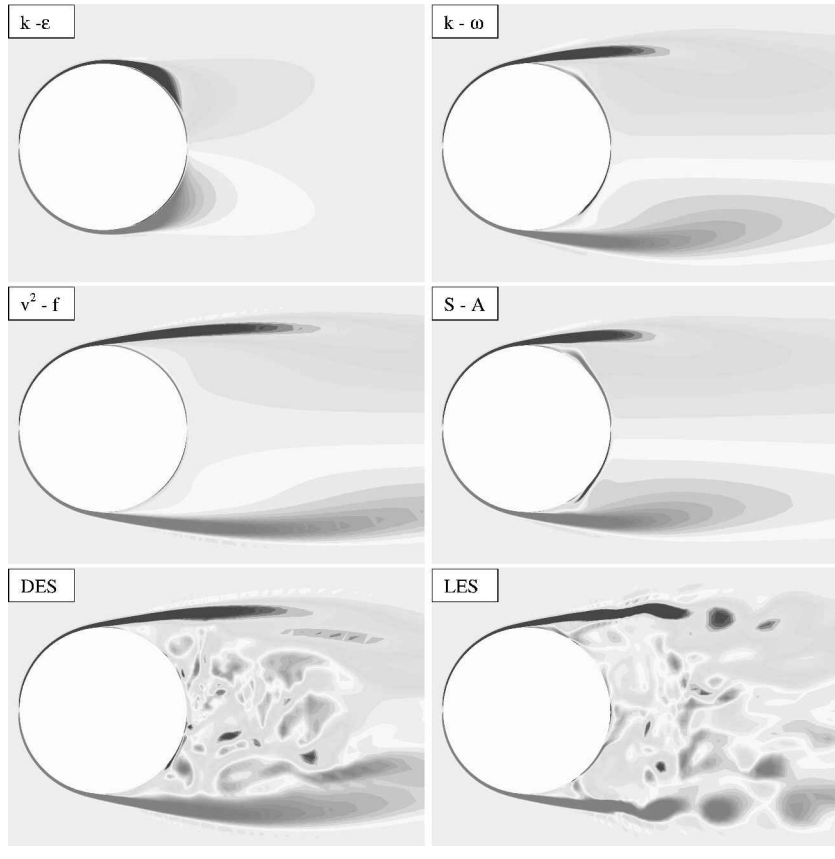

Fig. 4 Out-of-plane vorticity contours in an azimuthal plane: 24 increments in the contour levels from −10 to 10 U/D.

apparent in visualizations. In the recirculation region, a large number of smaller-scale eddies, nonexistent in the URANS calculations, are observed in the vorticity field from the DES and LES, which are able to resolve eddies down to the grid scale.

The RANS models, on the other hand, suppress the smaller eddies and, in general, reduce the three-dimensionality of the flow. With the exception of the k–ε model, the shear layers computed by the use of the different models are somewhat similar to the LES/DES, but with a smoother distribution of the vorticity in the recirculation region. As will be apparent later, the URANS predictions evolve to nearly steady and axisymmetric solutions. The Kelvin–Helmholtz instabilities that develop into vortex rings in the near wake must be modeled by the RANS closures. In general, the scale of the detached shear layers and range of vorticity values recorded in these regions are comparable in the URANS, LES, and DES calculations. Results obtained with $\overline{v^2}$–f predict the most elongated shear layers and are closest to the LES and DES visualizations.

URANS predictions of the mean streamwise drag coefficient C_d and rms value, back pressure coefficient $C_{p,\theta=180}$, main shedding frequency Strouhal number, the separation angle ϕ_s, and the transition angle ϕ_t, are summarized in Table 1. The transition angle as predicted by various models is calculated with a "turbulence index," a measure of when the closure model becomes active.[7] For the S–A model, the turbulence index is defined as $\partial\tilde{\nu}/\partial r/(\kappa u_\tau)$ where u_τ is the friction velocity. For the other models, the eddy viscosity was used in the evaluation, and, though a more coarse approximation, the aim was only to use the evaluation to deduce the range of rapid increase indicating the activation of the model.

As shown in Table 1, most of the RANS models are in reasonable agreement with the measurements of Achenbach[20] and Sakamoto and Haniu,[34] as well as the LES and DES predictions. The two-layer k–ε predictions are poor, an expected result given that the length scale prescription in the near-wall region is appropriate for fully turbulent boundary layers. Application of the two-layer model to the laminar sphere boundary layers severely damages predictions by this model. Table 1 also shows that the pressure recovery in the aft region is overpredicted by the RANS models, whereas the unsteadiness of the flow is better represented in the LES/DES and reflected in the improved prediction of $C_{p,\theta=180}$.

The reasonable predictions of C_d summarized in Table 1 with LES, DES, and the k–ω model, when compared to experimental data, might indicate the superiority of these models. However, uncertainities in the experimental measurements are not available, and it is important to remark that a different set of experimental measurements might favor one of the other closures. As will also be subsequently shown, k–ω calculations evolve to essentially steady flows without vortex shedding. It is not clear whether this result is specific to the moderate Reynolds number considered in this study, or whether shedding solutions might be apparent at higher Reynolds numbers where there is a larger-scale separation between the shed vortices and finer-scale turbulence.

With the exception of k–ε results, boundary-layer separation in all simulations occurs at around 85.5 ± 1.5 deg, slightly later than the value of 82.50 deg measured by Achenbach.[20] The 2–3-deg azimuthal variation of ϕ_s in the LES and DES predictions is a consequence of the shedding. Achenbach[20] did not report variations in ϕ_s in time or along the separation line and, consequently, it is not possible to report the rms variation in Table 1. The turbulence index used to calculate the polar angle interval corresponding to the transition region at the sphere surface is well defined with the S–A model (and, therefore, also DES). For the other closures, an approximate method was used. DES and S–A predictions of ϕ_t are practically the same and are also close to that obtained with k–ω. LES and $\overline{v^2}$–f seem to predict an earlier transition, immediately following separation at 87 deg. Finally, for the k–ε model, transition begins at approximately the same angle as separation. Though no experimental data are available for the location of the transition region, the models (except k–ε) correctly predict a subcritical flow at $Re = 10^4$ as $\phi_s < \phi_t$.

Figures 2 and 3 show the distribution of the mean pressure coefficient C_p and skin-friction coefficient C_f over the sphere. The results are averaged in time and spatially over the azimuthal direction. In Figs. 2 and 3, the symbols represent the experimental measurements for the subcritical flow at $Re = 1.62 \times 10^5$ (Ref. 20). Because the mean drag and flow physics are somewhat similar over the range of Reynolds numbers in the simulations and measurements, important differences between the present calculations at $Re = 10^4$ and the available set of experimental data are not expected. The agreement between simulation and experiment is quite good in the acceleration and part of the deceleration region for all simulations, with the exception of the k–ε results. The relative increase in the pressure coefficient near the aft region of the sphere is most accurately captured in the DES and LES. The k–ω distribution is also close to the measurements, except near the downstream stagnation point where the relative increase in C_p is clearly higher than the one occurring in the experimental measurements and DES/LES results. The same trend, more pronounced, is apparent in the S–A prediction. Results obtained with $\overline{v^2}$–f provide an improved prediction in the aft region compared to the other URANS models. The k–ε predictions more closely resemble a supercritical solution, though the drag prediction for the supercritical flow at higher Reynolds numbers is around 0.2, lower than the k–ε result of 0.291 (cf., Table 1).

The distributions of the skin friction from the LES, DES, and $\overline{v^2}$–f results are in good agreement with measurements (Fig. 3). Note that the $Re^{0.5}$ scaling of the skin friction in Fig. 3 is appropriate for the subcritical regime with laminar boundary-layer separation from

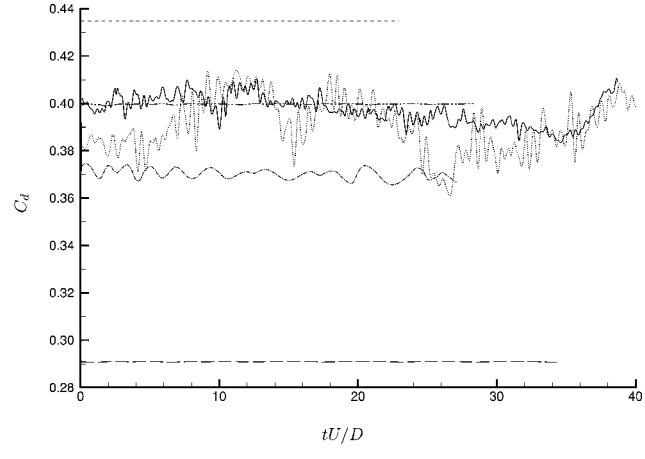

Fig. 5 Temporal variation of streamwise drag coefficient: – – –, k–ε; –···–, k–ω; –·–, $\overline{v^2}$–f; - - - -, S–A; · · · ·, LES; and ——, DES-CG.

Table 1 Effect of turbulence model on flow parameters

Model	C_d	$C_{p,\theta=180}$	Sr	ϕ_s, deg	ϕ_t-deg
k–ε	$0.291 \pm 7.70 \times 10^{-5}$	0.096	0.180	103.0	101–109[a]
k–ω	$0.400 \pm 1.56 \times 10^{-4}$	−0.132	0.210	86.5 ± 0.5	92–110[a]
$\overline{v^2}$–f	$0.370 \pm 2.08 \times 10^{-3}$	−0.207	0.220	86.0	87–88[a]
S–A	$0.435 \pm 2.12 \times 10^{-5}$	−0.165	0.220	87.0	93–108
LES	$0.393 \pm 1.43 \times 10^{-2}$	−0.229	0.195	85.0 ± 1.0	86–88[a]
DES	$0.397 \pm 7.00 \times 10^{-3}$	−0.277	0.200	85.5 ± 1.5	93–108
Experiment	0.40 ± 0.01	−0.28	——	0.195	82.5

[a]Calculation of ϕ_t using an approximate method.

the sphere. Based on the measurements, the skin friction is mildly overpredicted in these particular simulations for $90 < \phi < 140$ deg and mildly underpredicted for $140 < \phi < 180$ deg, although, as remarked earlier, the accuracy of the experimental measurements was not reported. These differences are accentuated in the k–ω results, as well as the prediction obtained with S–A, which shows a deeper minimum around $\phi = 160$ deg. Overall, all models (except k–ε) adequately predict the growth and separation of the boundary layers, with the turbulence models remaining dormant in the sphere boundary layers. Transition to turbulence in the present simulations occurs via the tripless mode.[11] Nonzero values of the eddy viscosity are convected from downstream and ignite the turbulence model in the separating shear layers.

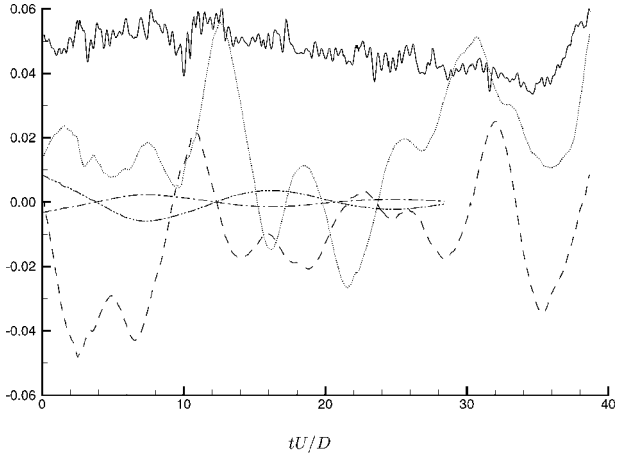

Fig. 6 Temporal variation of lateral force coefficients: ····, y component DES; – – –, z component DES; –·––, y component k–ω; –·–, z component k–ω; and ——, C_d for DES-CG (with vertical offset of 0.35).

The temporal variation of the drag coefficient in the k–ε, k–ω, and S–A results in Fig. 5 show virtually no departure from the average value, with a corresponding rms C_d of nearly zero. The v^2–f prediction, which shows a more visible temporal variation and for which the rms C_d is 0.0021, is nevertheless nearly an order of magnitude lower than that obtained with LES or DES. Based on this result, for the flow around the sphere at $Re = 10^4$, the v^2–f predictions of time-dependent features of chaotic unsteady flows appear superior to the other RANS models. Compared to the RANS results, the rms C_d is substantially greater in LES and DES. Resolution of the large eddies and alternate vortex shedding in these calculations are responsible for the larger deviations from the average drag (cf., Table 1 and Fig. 5). The effects of vortex shedding and its resolution by the simulation techniques are also illustrated in Fig. 6, where the time history of lateral-force coefficients is shown for DES and k–ω. There are important differences in the magnitude and nature of the lateral forces between the DES and the RANS prediction. (The LES results are similar and not shown.) Lateral forces in the RANS are small, whereas DES predicts a more significant variation around the mean with no regular pattern, consistent with the random nature of the shedding, and in agreement with observations from experiments. The nearly zero side forces predicted from the RANS are also consistent with the nearly axisymmetric solutions to which these calculations evolve. Figure 6 also shows that the frequency associated with the lateral-force variation is roughly two times lower than the shedding frequency in the time variation of the drag. This effect is also apparent in the URANS, though the rms values of the lateral force coefficients are close to zero. Note also that there are no peaks at higher frequencies in the DES histories

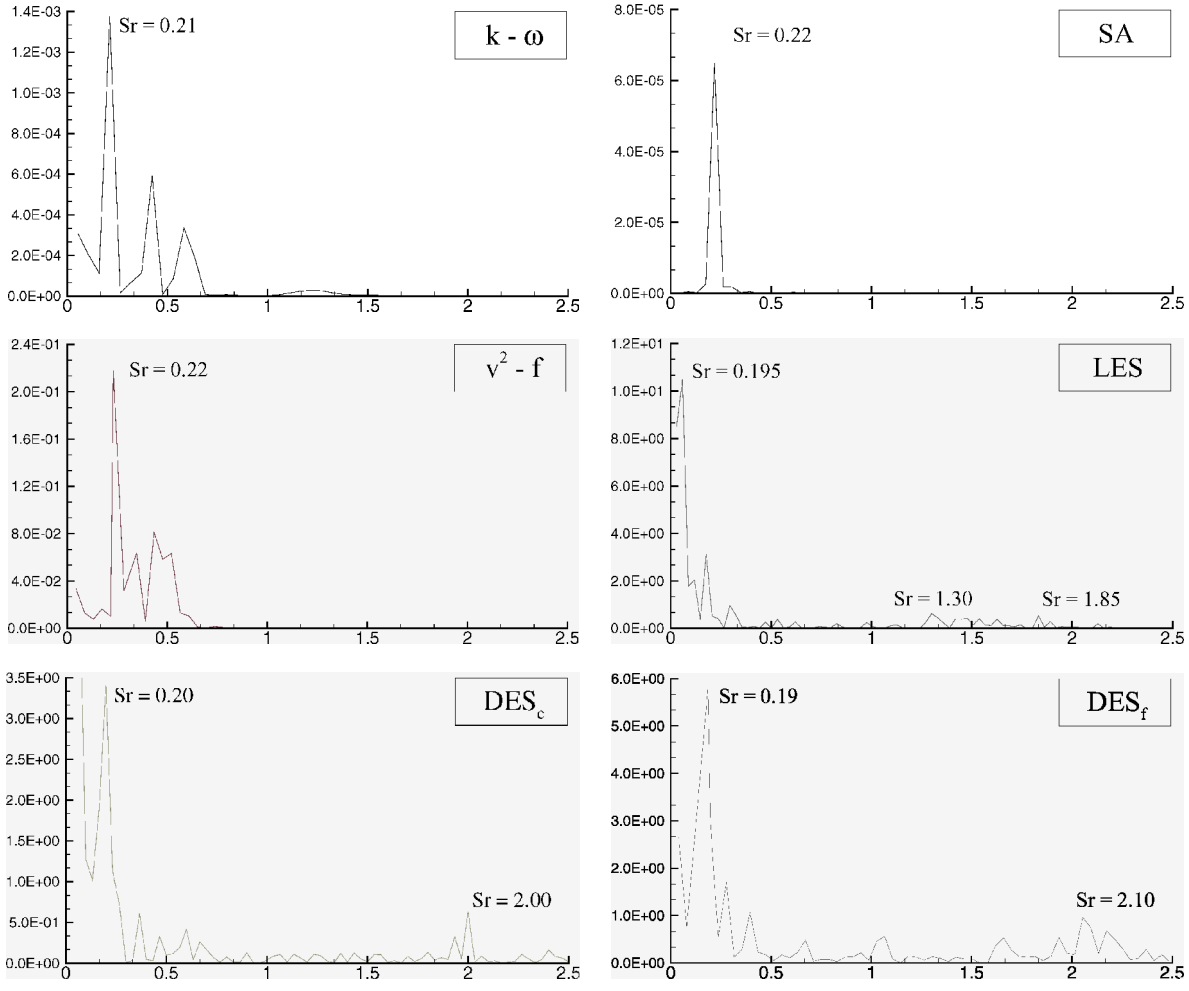

Fig. 7 Power spectra of the streamwise drag coefficient.

(nor in the LES histories not shown in Fig. 6). The higher frequency component evident in the C_d histories arises from the formation of Kelvin–Helmholtz instabilities in the detached shear layers (see Refs. 34 and 38). In the flow past a sphere, the vortices that form in these shear layers are vortex rings, approximately perpendicular to the main flow direction. The induced force and perturbations in the shed structures will then be primarily in the streamwise direction with the higher-frequency variations consequently more apparent in the streamwise force.

Predictions of the shedding frequencies (Table 1) are within 10% of the experimental measurements of Sakamoto and Haniu,[34] $Sr = 0.195 \pm 0.005$, for all simulations, with LES and DES yielding the best agreement. Wake frequencies were obtained by calculation of the power spectrum of the streamwise drag variation. Figure 7 shows that there is a clear maximum around the aforementioned value of the Strouhal number in each simulation. The vertical scale shows the energy content in the DES and LES predictions is characterized by a considerably larger amplitude compared to the URANS results, with the exception of v^2–f, where the energy content is about an order of magnitude smaller

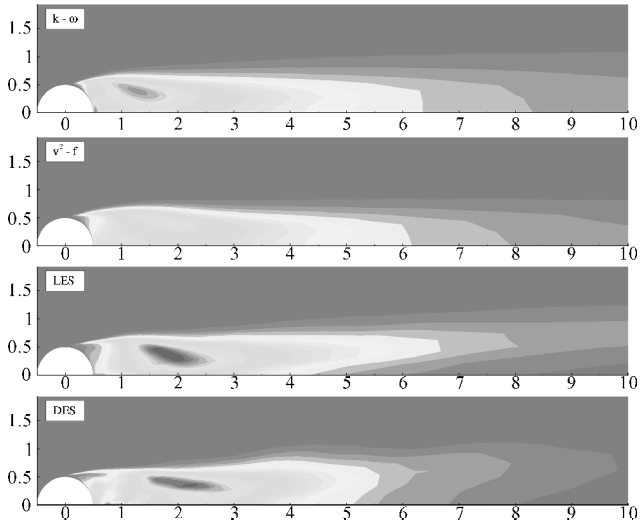

Fig. 8 Contours of turbulence kinetic energy: 25 increments in the contour levels from 0 to 0.08 K/U^2.

than in the DES and LES. Other maximums are also apparent near the main peak in Fig. 7, similar to the DNS results at $Re = 10^3$ of Tomboulides et al.[16] The LES and DES time histories of C_d and of their power spectra are also qualitatively similar in the sense that a second high-frequency band is captured between $Sr = 1.30$ and 1.85 in the LES, and between $Sr = 1.90$ and 2.10 in the DES. Sakamoto and Haniu[34] indicated a Strouhal number between 1.8 and 2.5 for the high-frequency mode at $Re = 10^4$. The high-frequency band predicted in the LES shows a possibly better capture than in the DES of the development of Kelvin–Helmholtz instabilities in the detached shear layers. The high-frequency component is not present in any of the RANS results, indicative of these motions being parameterized by the turbulence model. Though the Strouhal number of the high-frequency component is somewhat underpredicted compared to measurements, the present results would indicate that LES/DES adequately predicts the dynamics of the vortex shedding process.

Contours of the turbulence kinetic energy K are shown in Fig. 8. The distributions shown are obtained when the times are averaged over at least six shedding cycles and spatially averaged over the azimuthal direction. (When the DES solution was averaged over 12 shedding cycles, a negligible change in the statistics was yielded.) Only the resolved turbulent kinetic energy is shown in Fig. 8 for the LES and DES predictions. Figure 8 shows that all calculations capture the pocket of high K behind the sphere in the recirculation region, where the level of the turbulent shear stresses (not shown) are also large (due to the distortion of the mean flow and associated increase in turbulence production). DES and LES predictions agree reasonably well with one another, both qualitatively as well as quantitatively. The k–ω predictions are roughly similar to the LES and DES results, though there Fig. 8 shows that the region of highest kinetic energy levels is closer to the sphere, at around $x/D = 1$, rather than $x/D = 2$ as in the LES and DES. The v^2–f predictions compare favorably with LES and DES in that the region of elevated K are closer than for k–ω, though the actual values in the region of high kinetic energy are about 30% lower. In addition, RANS predictions of kinetic energy levels are also higher in the detached shear layers compared to LES/DES.

Eddy viscosities from the RANS and subgrid viscosities for the LES and DES are shown in Fig. 9. The lower levels in the wake for the LES and DES, as compared to the RANS results, are a consequence of most of the turbulent stress being resolved (about 90% of the total stress) in these simulations, whereas for the RANS, all of the stresses are modeled. For similar mean flows, the level of the

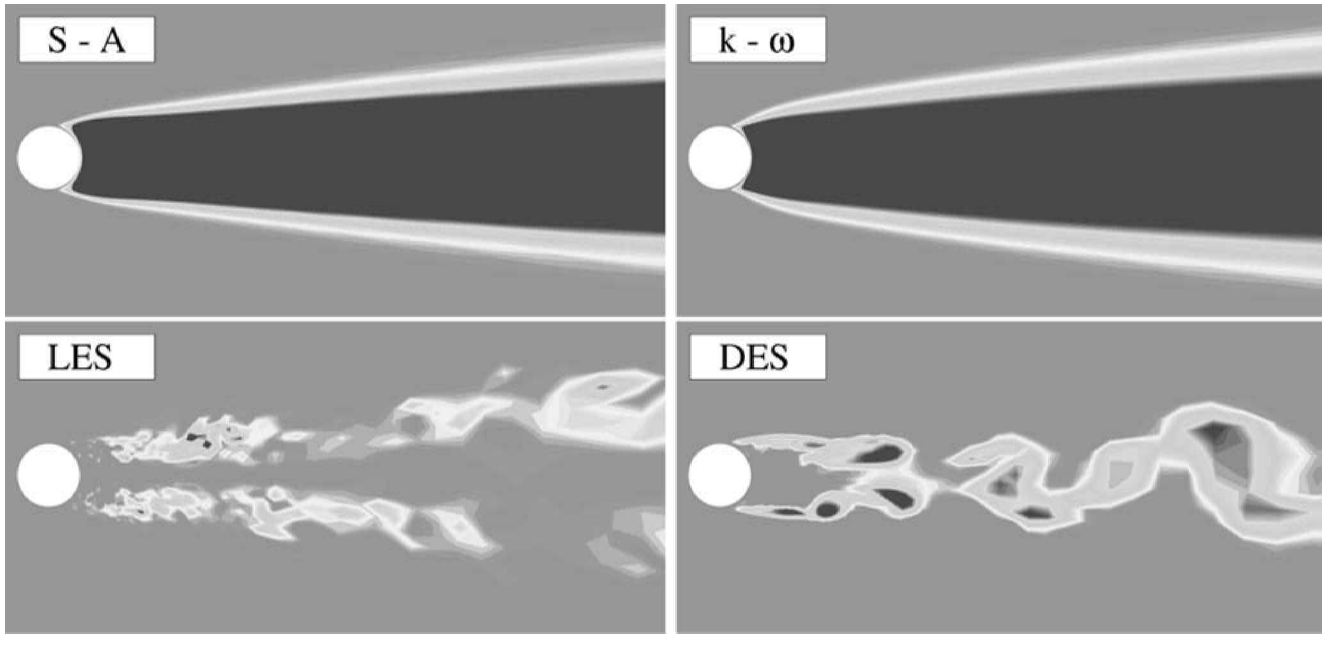

Fig. 9 RANS eddy-viscosity and LES/DES subgrid viscosity in the sphere wake: 25 increments in the contour levels from 0 to 25 ν_t/ν.

turbulent stresses can be roughly deduced from the magnitude of ν_t. Though not shown here, the distributions of the averaged turbulent stresses are similar for all of the techniques and, consequently, the URANS eddy viscosity for the present simulations should be about one order of magnitude higher than the SGS viscosity in the LES or DES, in agreement with Fig. 9. The qualitative differences in the instantaneous distributions between LES/DES and URANS calculations is again a consequence of the large eddies being resolved in the LES/DES and the SGS viscosity levels in these turbulent regions being higher than in the surrounding flow. In the URANS cases, the distribution of ν_t reflects the time-averaged values in the wake where the shedding is not well represented. The URANS results also exhibit the region of highest eddy viscosity in the recirculation region, while DES and LES results show the correlation with shed structures in the wake. In the detached shear layers, RANS eddy viscosities are predictably high, while the structures are mostly resolved in the LES and DES.

IV. Summary

URANS methods were applied to prediction of the flow over a sphere at $Re = 10^4$. One-, two-, and four-equation isotropic eddy-viscosity turbulence models were employed, with results compared to experimental measurements and predictions from LES and DES. The flow experienced laminar boundary-layer separation with transition to turbulence occurring via the development and breakdown of Kelvin–Helmholtz instabilities in the detached shear layers.

With the exception of the two-layer k–ε model, URANS predictions of the pressure coefficient, skin friction, and (by association) the streamwise drag, were in reasonable agreement with measurements. Predictions of turbulence kinetic energy and the shear stress were similar to LES and DES results. The relative accuracy of the URANS in predicting this flow was somewhat unexpected because two-dimensional URANS typically results in large overpredictions of the drag.[11] URANS solutions did not, however, adequately resolve shedding mechanisms, leading to a poor prediction of wake frequencies and especially the energy associated with the main instability modes. This behavior is unlike URANS of the circular cylinder where the main shedding is more prominently represented. This difference in the character of RANS solutions for the sphere and cylinder might be explained in part by the wavelengths most responsible for the main shedding and the ability of a model to capture them.

The k–ω predictions of the pressure and skin-friction coefficients, the mean drag, and the position of the laminar separation location were in closest agreement with LES and DES, but rms variations in the drag and lateral forces were essentially zero. Results obtained by the use of v^2–f for these quantities were also satisfactory. Predictions of the unsteady features of the flow with v^2–f were superior compared to the other models, for example, the amplitude of the drag coefficient variations were the highest, though still sensibly lower than those in the LES and DES. The S–A model predicted a somewhat higher mean drag coefficient, whereas the rms value of the drag was the smallest of all of the RANS models. These findings should be considered also in the context of computational cost, that is, the S–A runs were the most efficient in view of CPU considerations and yield acceptable predictions of integral quantities such as C_p, C_f, and C_d.

The improved comparison against experimental measurements from the LES and DES relative to the RANS results is related in large part to the vortex shedding process being mostly resolved, rather than modeled. Details of the shedding that must be accounted for in a RANS model are difficult to parameterize accurately. For applications in which time-dependent information is crucial, techniques such as LES and DES are advantageous. LES predictions that use the dynamic eddy-viscosity model exhibited less SGS dissipation and consequently yielded more energetic turbulent solutions. The relatively better performance of the LES compared to the DES is consistent with the DES solutions being obtained with a suboptimal subgrid model, that is, one that is constrained by the RANS calibration inherent to S–A. In addition, for the laminar boundary-layer separation considered in this study, DES predictions constitute an LES performed with a one-equation transport model for the subgrid viscosity and do not fully test the capabilities of the method. Supercritical flows with turbulent boundary-layer separation introduce more empiricism and strongly challenge feature-resolving techniques such as LES and DES. At high Reynolds numbers, LES predictions will require a different treatment of the wall layer, whereas DES predictions in flows with turbulent boundary-layer separation will be more sensitive to RANS modeling approximations in predicting boundary-layer growth and separation.

Acknowledgments

This work is supported by the U.S. Office of Naval Research (Grants N00014-96-1-1251, N00014-97-1-0238, and N00014-99-1-0922, Program Officers L. P. Purtell and C. Wark). The authors gratefully acknowledge valuable discussions with P. R. Spalart.

References

[1]Spalart, P. R., "Strategies for Turbulence Modeling and Simulations," *International Journal of Heat and Fluid Flow*, Vol. 21, 2000, pp. 252–263.

[2]Rodi, W., "On the Simulation of Turbulent Flow past Bluff Bodies," *Computational Wind Engineering One: Proceedings of the 1st International Symposium on Computational Wind Engineering*, Elsevier Science, 1992, pp. 3–19.

[3]Durbin, P. A., "Separated Flow Computations Using the k–ε–v^2 Model," *AIAA Journal*, Vol. 33, No. 4, 1995, pp. 659–664.

[4]Chen, H. C., and Patel, V. C., "Near-Wall Turbulence Models for Complex Flows Including Separation," *AIAA Journal*, Vol. 26, 1988, pp. 641–648.

[5]Wilcox, D. C., "Reassessment of the Scale-Determining Equation for Advanced Turbulence Models," *AIAA Journal*, Vol. 26, 1988, pp. 1299–1310.

[6]Durbin, P. A., "Near-Wall Turbulence Closure Without Damping Functions," *Theoretical and Computational Fluid Dynamics*, Vol. 3, No. 1, 1991, pp. 1–13.

[7]Spalart, P. R., and Allmaras, S. R., "A One-Equation Turbulence Model for Aerodynamic Flows," *La Recherche Aerospatiale*, Vol. 1, 1994, pp. 5–21.

[8]Johansson, S., Davidson, L., and Olsson, E., "Numerical Simulation of the Vortex Shedding Past Triangular Cylinders at High Reynolds Numbers Using a k–ε Turbulence Model," *International Journal of Numerical Methods in Fluids*, Vol. 16, No. 6, 1993, pp. 859–878.

[9]Franke, R., and Rodi, W., "Calculation of Vortex Shedding past a Square Cylinder with Various Turbulence Models," edited by F. Durst, *Turbulent Shear Flows 8*, Springer-Verlag, New York, 1993, pp. 189–204.

[10]Bosch, G., and Rodi, W., "Simulation of Vortex Shedding past a Square Cylinder with Different Turbulence Models," *International Journal of Numerical Methods in Fluids*, Vol. 28, 1998, pp. 601–616.

[11]Shur, M., Spalart, P., Strelets, M., and Travin, A., "Navier–Stokes Simulation of Shedding Turbulent Flow past a Circular Cylinder and a Cylinder with a Backward Splitter Plate," *Computational Fluid Dynamics '96. Proceedings of 3rd European CFD Conference*, edited by J.-A. Desideri, C. Hirsch, and P. Le Tallec, Wiley, Chichester, England, U.K., 1996, pp. 676–682.

[12]Travin, A., Shur, M., Strelets, M., and Spalart, P. R., "Detached-Eddy Simulations past a Circular Cylinder," *Flow, Turbulence, and Combustion*, Vol. 63, 2000, pp. 293–313.

[13]Shur, M. L., Spalart, P. R., Strelets, M. K., and Travin, A. K., "Detached-Eddy Simulation of an Airfoil at High Angle of Attack," *Proceedings of the 4th International Symposium on Engineering Turbulence Modelling and Measurements*, edited by W. Rodi and D. Laurence, Elsevier, Amsterdam, 1999, pp. 669–678.

[14]Drikakis, D., "Development and Implementation of Parallel High Resolution Schemes in 3D Flows over Bluff Bodies," *Proceedings of Parallel CFD Conference—Implementation and Results Using Parallel Computers*, Elsevier Science, New York, 1995, pp. 191–198.

[15]Baldwin, B., and Lomax, H., "Thin Layer Approximation and Algebraic Model for Separated Turbulent Flows," AIAA Paper 78-257, Jan. 1978.

[16]Tomboulides, A. G., Orszag, S. A., and Karniakidis, G. E., "Direct and Large-Eddy Simulations of Axisymmetric Wakes," AIAA Paper 93-0546, Jan. 1993.

[17]Tomboulides, A. G., and Orszag, S. A., "Numerical Investigations of Transitional Weak Turbulent Flow past a Sphere," *Journal Fluid Mechanics*, Vol. 416, 2000, pp. 47–73.

[18]Chapman, D. R., "Computational Aerodynamics Development and Outlook," *AIAA Journal*, Vol. 17, No. 12, 1979, pp. 1293–1313.

[19]Spalart, P. R., Jou, W. H., Strelets, M., and Allmaras, S. R., "Comments on the Feasibility of LES for Wings, and on a Hybrid RANS/LES Approach," *Advances in DNS/LES: First AFOSR International Conference on DNS/LES*, edited by C. Liu and Z. Liu, Greyden, Columbus, OH, 1997.

[20]Achenbach, E., "Experiments on the Flow past Spheres at Very High Reynolds Numbers," *Journal of Fluid Mechanics*, Vol. 54, No. 3, 1972, pp. 565–575.

[21]Constantinescu, G. S., and Patel, V. C., "A Numerical Model for Simulation of Pump-Intake Flow and Vortices," *Journal of Hydraulic Engineering*, Vol. 124, No. 2, 1998, pp. 123–134.

[22]Constantinescu, G. S., and Patel, V. C., "Numerical Simulation of Flow in Pump-Bays Using Near-Wall Turbulence Models," Iowa Inst. of Hydraulic Research, IIHR Rept. 394, Univ. of Iowa, Iowa City, IA, 1998.

[23]Johnson, T. A., "Numerical and Experimental Investigation of the Flow Past a Sphere up to a Reynolds Number of 300," Ph.D. Dissertation, Dept. of Mechanical Engineering, Univ. of Iowa, Iowa City, IA, March 1996.

[24]Sotiropoulos, F., and Abdallah, S., "A Primitive Variable Method for the Solution of Three-Dimensional Incompressible Viscous Flows," *Journal of Computational Physics*, Vol. 103, No. 2, 1992, pp. 336–349.

[25]Sotiropoulos, F., and Patel, V. C., "Flow in Curved Ducts of Varying Cross-Section," Iowa Inst. of Hydraulic Research, IIHR Rept. 358, Univ. of Iowa, Iowa City, IA, 1992.

[26]Rajendran, V. P., Constantinescu, S. G., and Patel, V. C., "Experiments in Flow in a Model Water-Pump Intake Sump to Validate a Numerical Model," American Society of Mechanical Engineers, Paper FEDSM98-5098, June 1998.

[27]Wilcox, D. C., *Turbulence Modeling for CFD*, DCW Industries, Inc., La Canada, CA, 1993.

[28]Germano, M., Piomelli, U., Moin, P., and Cabot, W. H., "A Dynamic Subgrid-Scale Eddy Viscosity Model," *Physics of Fluids A*, Vol. 3, 1991, pp. 1760–1765.

[29]Meneveau, C., Lund, T., and Cabot, W., "A Lagrangian Dynamic Subgrid-Scale Model of Turbulence," *Journal of Fluid Mechanics*, Vol. 319, 1996, p. 353.

[30]Sotiropoulos, F., and Patel, V. C., "Prediction of Turbulent Flow Through a Transition Duct Using a Second-Moment Closure," *AIAA Journal*, Vol. 32, No. 11, 1994, pp. 2194–2204.

[31]Sotiropoulos, F., and Patel, V. C., "Application of Reynolds-Stress Transport Models to Stern and Wake Flows," *Journal of Ship Research*, Vol. 39, No. 4, 1995, pp. 263–283.

[32]Johnson, T. A., and Patel, V. C., "Flow past a Sphere up to a Reynolds Number of 300," *Journal of Fluid Mechanics*, Vol. 378, No. 1, 1999, pp. 19–70.

[33]Roos, F. W., and Willmarth, W. W., "Some Experimental Results on Sphere and Disk Drag," *AIAA Journal*, Vol. 9, No. 2, 1971, pp. 285–291.

[34]Sakamoto, H., and Haniu, H., "A Study of Vortex Shedding from Spheres in an Uniform Flow," *Journal of Fluids Engineering*, Vol. 112, 1990, pp. 386–392.

[35]Constantinescu, G. S., and Squires, K. D., "LES and DES Investigations of Turbulent Flow over a Sphere," AIAA Paper 2000-0540, Jan. 2000.

[36]Mittal, R., and Moin, P., "Suitability of Upwind-Biased Finite Difference Schemes for Large-Eddy Simulation of Turbulent Flows," *AIAA Journal*, Vol. 35, No. 8, pp. 1415–1417.

[37]Beaudan, P., and Moin, P., "Numerical Experiments on the Flow past a Circular Cylinder at Sub-Critical Reynolds Number," Dept. of Mechanical Engineering, Rept. TF-62, Stanford Univ., Stanford, CA, 1994.

[38]Taneda, S., "Visual Observations of the Flow past a Sphere at Reynolds Numbers Between 10^4 and 10^6," *Journal of Fluid Mechanics*, Vol. 85, 1978, pp. 187–192.

R. M. C. So
Associate Editor